



## OPEN

SUBJECT AREAS:  
NANOTECHNOLOGY IN  
CANCER  
CANCER IMAGINGReceived  
10 January 2014Accepted  
12 March 2014Published  
9 May 2014Correspondence and  
requests for materials  
should be addressed to  
A.S.B. (asbiris@ualr.  
edu) or V.P.Z.  
(zharovvladimirp@  
uams.edu)

# Circulating tumor cell identification by functionalized silver-gold nanorods with multicolor, super-enhanced SERS and photothermal resonances

Zeid A. Nima<sup>1</sup>, Meena Mahmood<sup>1</sup>, Yang Xu<sup>1</sup>, Thikra Mustafa<sup>1</sup>, Fumiya Watanabe<sup>1</sup>, Dmitry A. Nedosekin<sup>2</sup>, Mazen A. Juratli<sup>2</sup>, Tariq Fahmi<sup>3</sup>, Ekaterina I. Galanzha<sup>2</sup>, John P. Nolan<sup>4</sup>, Alexei G. Basnakanian<sup>3</sup>, Vladimir P. Zharov<sup>2</sup> & Alexandru S. Biris<sup>1</sup><sup>1</sup>Center for Integrative Nanotechnology Sciences, University of Arkansas at Little Rock, 2801 S. University Avenue, Little Rock, Arkansas 72204, USA, <sup>2</sup>Arkansas Nanomedicine Center, University of Arkansas for Medical Sciences, 4301 W. Markham St, Little Rock, Arkansas 72205, USA, <sup>3</sup>Department of Pharmacology and Toxicology, University of Arkansas for Medical Sciences, 4301 W. Markham St, Little Rock, Arkansas 72205, USA, <sup>4</sup>La Jolla Bioengineering Institute, San Diego, California, USA.

Nanotechnology has been extensively explored for cancer diagnostics. However, the specificity of current methods to identify simultaneously several cancer biomarkers is limited due to color overlapping of bio-conjugated nanoparticles. Here, we present a technique to increase both the molecular and spectral specificity of cancer diagnosis by using tunable silver-gold nanorods with narrow surface-enhanced Raman scattering (SERS) and high photothermal contrast. The silver-gold nanorods were functionalized with four Raman-active molecules and four antibodies specific to breast cancer markers and with leukocyte-specific CD45 marker. More than two orders of magnitude of SERS signal enhancement was observed from these hybrid nanosystems compared to conventional gold nanorods. Using an antibody rainbow cocktail, we demonstrated highly specific detection of single breast cancer cells in unprocessed human blood. By integrating multiplex targeting, multicolor coding, and multimodal detection, our approach has the potential to improve multispectral imaging of individual tumor cells in complex biological environments.

Most cancer deaths are related to metastasis in various organs due to the hematogenous dissemination of circulating tumor cells (CTCs)<sup>1–3</sup>. Clinical studies have shown that the CTCs can be used as a marker of metastatic development, survival time, (the lower the CTC count, the longer the survival time), cancer recurrence, and therapeutic efficacy<sup>3–6</sup>. The invasion of the circulation by tumor cells may occur very early underscoring the need for the sensitive detection of CTCs. A variety of assays have been developed to detect CTCs in a sample of peripheral blood: reverse transcription–polymerase chain reaction (RT-PCR), optical detectors, negative selection, cell-size filtration, CellSearch<sup>TM</sup> (Veridex LLC), and microfluidic chip techniques (e.g., iChip), among many others<sup>1–6</sup>. However, most of these methods will require optimization prior to large-scale clinical applications. Most assays also have limited capacity for targeting CTCs by simultaneously using several molecular markers. CellSearch<sup>TM</sup>, an FDA-approved CTC assay, and several microfluidic chip-based assays (e.g., CTC-iChip) use markers with immune-magnetic beads to isolate CTCs on the basis of EpCAM expression<sup>3,5,6</sup>. The isolated CTCs are further distinguished by their labeling with keratin, DAPI, while CD45 was used as the positive marker for white blood cells (WBCs).

Nanotechnology has been extensively explored for ultrasensitive detection of CTCs. Combinations of multifunctional nanosystems and optical methods have demonstrated an ultimate sensitivity at the level of a single cell that is important for early cancer diagnosis<sup>7–10</sup>.

However, most CTC assays have rather low specificity due to the limited cancer biomarker used (e.g., EpCAM and/or keratin) and the overlapping, relatively broad absorption and emission spectra of existing nanoparticles or fluorescent tags<sup>10–14</sup>. In addition, most CTC assays require multiple time-consuming processes (e.g., labeling, immunomagnetic isolation, red blood cell [RBC] and WBC separation) that may result in substantial (up to 60–95%) loss of CTCs. Multifunctional nanoparticles conjugated with antibodies, folates, aptamer, or other ligands were proposed and successfully used for selective targeting, imaging, and treatment of CTCs using fluorescence,



photothermal (PT), SERS, and other spectral methods<sup>7–26</sup>. However, their multiplex capabilities are generally limited by relatively broad absorption and emission spectral characteristics. In particular, quantum dots (QDs) while providing a wide variety of fluorescent colors have limited use due to a significant auto-fluorescence background of blood and the presence of various fluorescent artifacts<sup>12–14</sup>.

An interesting approach for multiplex visualization clearly indicated the ability to use various Raman active fingerprints for SERS-based analysis in animal models<sup>27</sup>. This study demonstrated drastically higher *in vivo* detection sensitivity for the SERS nanostructures compared to classical QDs (picomolar vs. nanomolar).

Here, we introduce a new approach for the highly specific multiplex targeting and multicolor identification of tumor cells in unprocessed whole human blood using silver-coated gold nanorods (AuNR/Ag) to avoid any undesired CTC losses. The strong absorption and plasmonic amplification of the corresponding Raman signal by AuNR/Ag enhances spectral identification of cells, based on the narrow SERS spectral lines and spectral PT signatures<sup>7</sup>. These characteristics make such bi-metal nanorods excellent candidates for multimodal SERS-PT tumor cell detection and identification since they can overcome the limitations related to sample auto-fluorescence.

## Results

To create unique spectral-molecular signatures, the AuNR/Ag were divided into four families, each being conjugated with a unique organic

Raman molecule (4-mercaptobenzoic acid [4MBA], *p*-aminothiophenol [PATP], *p*-nitrothiophenol [PNTP], and 4-(methylsulfanyl) thiophenol [4MSTP]) having different SERS spectra and a different antibody specific for four breast cancer markers: Anti-Epithelial Cells Adhesion Molecules (Anti-EpCAM)<sup>25</sup>, Anti-CD44<sup>23,24</sup>, Anti-Keratin18<sup>20</sup>, and Anti-Insulin-like growth factor antigen (Anti-IGF-I Receptor  $\beta$ )<sup>17,18</sup> (Fig. 1A–C).

We chose these antibodies as targeting molecules for our SERS agents for the following reasons: EpCAM has been used extensively in breast cancer detection because this antibody is greatly over-expressed in a plethora of cancers, including colon, liver, pancreatic, prostate, and breast cancer<sup>25</sup>. Since EpCAM is highly expressed in adeno carcinomas and squamous cell carcinomas and the MCF-7 cells originating from these cells, they express a considerable amount of EpCAM antigen on their surface. CD44 is a cell-cell and cell-matrix adhesion molecule known to be highly expressed in many types of cancers and is therefore frequently used for the diagnosis and prognosis of breast cancer<sup>23,24</sup>. The importance of CD44 in tumor development and progression has been widely discussed and provides multiple prospects for advanced cancer treatments by targeting therapeutics to the CD44 receptor of metastatic tumors, and interfering with the CD44 signaling pathway<sup>21,22</sup>. Anti-Keratin 18 antibodies have been used in the diagnostic histopathology of breast cancer for more than two decades. It is known to be highly expressed in normal mammary epithelial cells, and MCF-7 cells, which are adenocarcinoma cells derived from breast epithelium<sup>20</sup>. In addition,

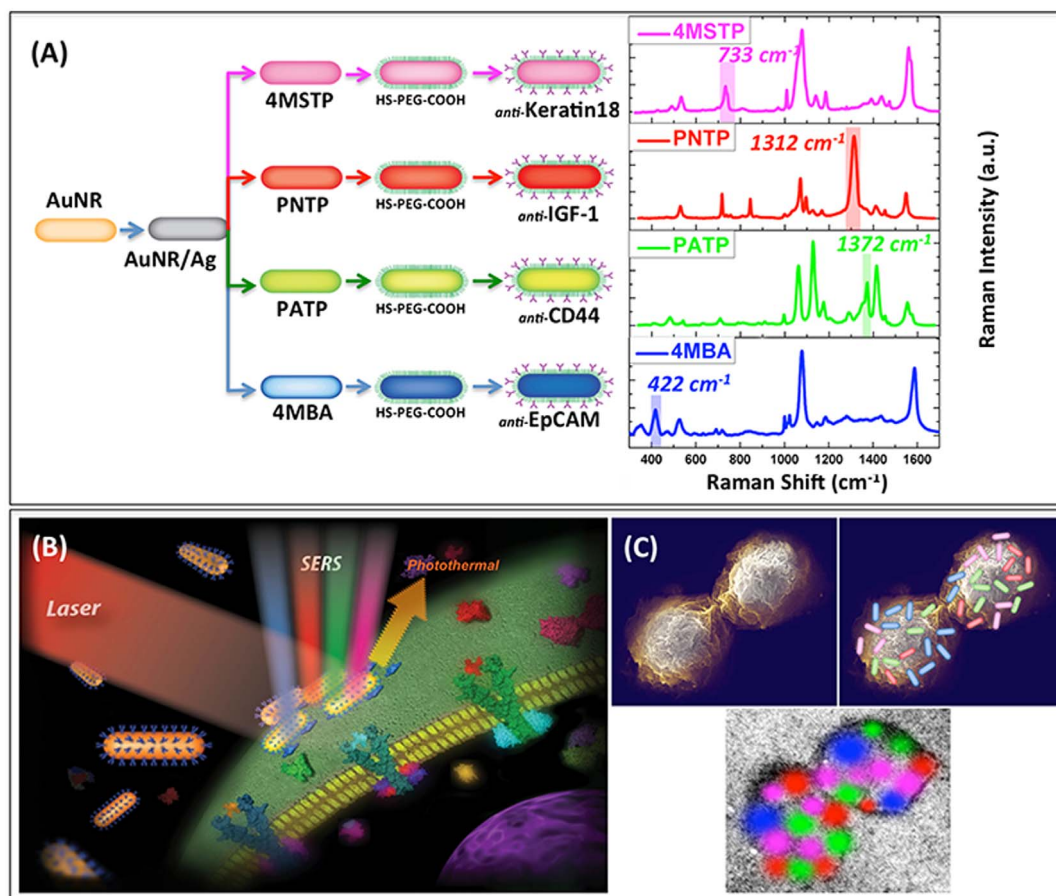


**Figure 1** | (A) Schematic diagram (preparation steps) and Raman spectra (acquisition time 50 s) for the four families of SERS nano-agents. A color was assigned to a non-overlapping peak from each SERS spectrum as follows: Blue: AuNR/Ag/4MBA/*anti*-EpCAM, Red: AuNR/Ag/PNTP/*anti*-IGF-1 Receptor  $\beta$ , Green: AuNR/Ag/PATP/*anti*-CD44, Magenta: AuNR/Ag/4MSTP/*anti*-Keratin18. Abbreviations are as follows: 4MBA = 4-mercaptobenzoic acid, PNTP = *p*-nitrobenzoic acid, PATP = *p*-aminothiophenol, 4MSTP = 4-(methylsulfanyl) thiophenol. (B) Schematics of breast cancer cell surface targeting by four nano-agents and SERS/PT detection technique. (C) Schematics of 2D multi-color SERS data correlation with nano-agents' distribution on cell surface.



it has been shown that the down-regulation of membrane Keratin 18 plays a key role in the prognosis of the breast cancer<sup>19</sup>. Finally, IGF-I has been shown to be expressed in 90% of breast cancer specimens<sup>17,18</sup>; therefore, the anti-IGF-I Receptor  $\beta$  antibody was used as another molecule to target breast cancer cells along with the gold nanorods<sup>28,29</sup>.

Our approach of using four antibodies with four detection SERS nanoparticle signatures was based on the goal of dramatically increasing the specificity of detection of a particular type of CTCs and reducing the undesired false readings. Having multiple (four, in our case) targeting and detection signatures overlapping over one cell would therefore result in a highly enhanced level of detection specificity by rejecting false positive readings resulting from only one or two of the expected molecular signatures.

Molecular targeting of tumor cells with the antibody rainbow cocktails was verified with PT and SERS imaging and spectroscopic techniques. The selected SERS peak of each of the four organic molecules (e.g., at  $422\text{ cm}^{-1}$  for 4MBA,  $1372\text{ cm}^{-1}$  for PATP,  $1312\text{ cm}^{-1}$  for PNTP, and  $733\text{ cm}^{-1}$  for 4MSTP) did not overlap with the others and was coded by the following colors: blue for 4MBA, green for PATP, red for PNTP, and magenta for 4MSTP (Fig. 1A). Furthermore, the four color-coded SERS signatures were multiplexed with the PT microscopy (PTM) signatures used for the two-dimensional (2-D) imaging. Once the spectroscopic signatures were collected, they were superimposed onto the optical image, resulting in enhanced specificity for the detection of a single tumor

cell in blood—thereby reducing the possibility of false-negativity and false-positivity. The final result included the integration (or “painting”) of four highly specific SERS-based colors along with their PT signatures over the optical image of each tumor cell (Fig. 1B).

For the construction of these multiplex spectroscopic nanoagents, we used a layer-by-layer approach, as previously presented<sup>30</sup>, as shown in Supplementary Fig. S1. First, around 90% of prepared gold nanorods (AuNRs) having an aspect ratio (AR) of around  $3.00 \pm 0.23$  were synthesized and then subsequently covered by an Ag layer with a thickness of around  $1.70 \pm 0.30\text{ nm}$  (Supplementary Fig. S2), resulting in the formation of AuNR/Ag hybrid contrast agents. Transmission electron microscopy (TEM) images (Fig. 2A (a1)–(a5) and Supplementary Fig. S3–S4) revealed that the AuNRs’ length and diameter were approximately  $36.00 \pm 0.80\text{ nm}$  and  $12.00 \pm 0.41\text{ nm}$  with longitudinal plasmon resonances at around  $766\text{ nm}$  (Fig. 2C)—close to the excitation laser wavelength used ( $785\text{ nm}$ ). The silver shells’ growth on the gold nanorod surfaces was confirmed by the absorbance spectra (as shown in Fig. 2C). After the silver shell growth, the longitudinal band of gold nanorods showed a blue shift of around  $20\text{ nm}$  ( $740\text{ nm}$ ), with no Ag-specific peak being observed, indicating that the very thin layer of Ag completely covered the surface of the AuNRs<sup>31</sup>. These observations were additionally confirmed by TEM (Fig. 2A) and STEM images (Fig. 2B). When the 4MBA was adsorbed over the AuNRs’ surface, we measured a SERS enhancement factor of approximately 6 times, compared to the 4MBA solution, alone. For AuNR/Ag nanostructures, a 129-fold SERS signal enhancement

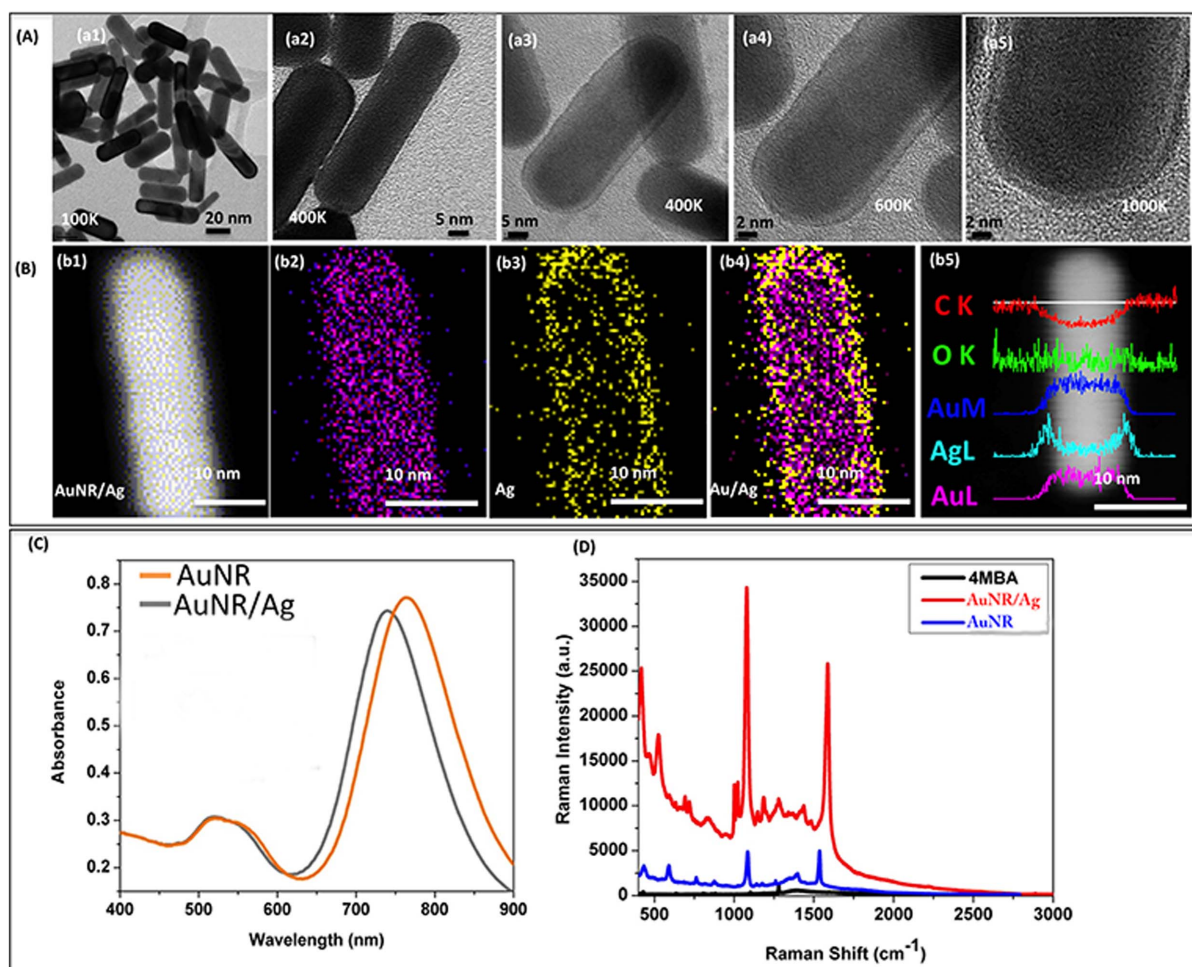


**Figure 2** | (A) (a1–a2) High resolution transmission electron microscopy (HR-TEM) images of pure gold Nanorods (AuNRs); (a3–a5) HRTEM images of AuNR/Ag. (B) (b1–b4) STEM and EDS elemental mapping images for AuNR/Ag nanorods; (b5) EDS cross-scanning spectra for the AuNR/Ag nanorods. (C) Optical absorption spectra for AuNR and AuNR/Ag structures. (D) Raman scattering intensity for 4MBA (10 mM), and 4MBA deposited on AuNRs and AuNR/Ag (acquisition time 10 s).

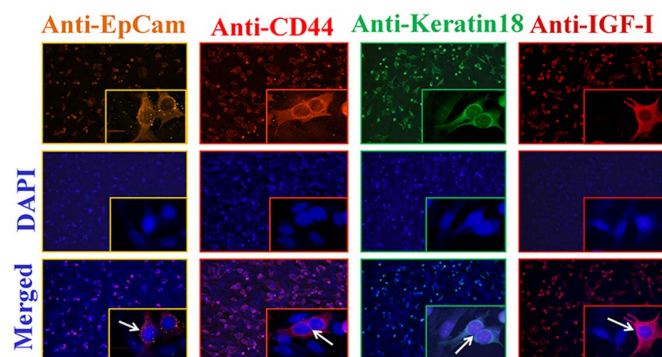


**Figure 3** | Immunocytochemistry staining (ICC) of MCF-7 cells in a mixed culture with fibroblast BJ-1 cells. Top row, anti-EpCAM, anti-CD44, anti-Keratin 18, and anti-IGF antibodies (1:200) staining of cells followed by (1:500 of dilution) goat anti-mouse IgG (Alexa fluor 555, 594, 488, and 647), respectively. Middle row, DAPI nuclear stainings. Bottom row, merged images of two upper rows. The white arrows indicate surface labeled MCF-7 cells, while fibroblast cells are not labeled.

compared to that of pure AuNRs (Fig. 2D) was achieved when decorated with 4MBA, which is in excellent correlation with the already presented results<sup>32</sup>. Therefore, the addition of the Ag layer resulted in a significant increase in the enhancement factor for the Raman spectrum corresponding to the organic molecule. This finding directly impacts our detection technology since more intense SERS signals are translated in lower detection times and with higher sensitivity. It is important that the antibody-covered multispectral

SERS nanorods retained their strong optical absorption at longitudinal and transversal plasmon resonances (Supplementary Figs. S5, S6).

Additionally, these complex nanorod structures are excellent super-contrast PT agents<sup>7</sup> having absorption maxima in the near infra-red spectral range corresponding to the minimum of biological tissues absorbance. Both conventional optical absorption (Fig. 2C) and PT spectra of the particles (Supplementary Fig. S7) had maximum at ~730–750 nm with a slight red-shift in absorption maxima observed for large clusters. The narrow PT spectra<sup>7</sup> and high PT contrast of the nanorods without notable influence from the thin Ag layer, may be used for rapid sample screening using PT microscopy followed by SERS analysis with unique spectral fingerprints. We foresee a further increase in the number of SERS colors/biomarkers for molecular tumor cell detection up to an estimated 6–8 in order to further enhance the detection sensitivity and specificity.

To evaluate the biological utility of this platform, we discriminated two cell lines--breast cancer (MCF-7) and fibroblast--using immunocytochemistry for verification of molecular targeting by adding secondary antibodies conjugated with fluorescent dyes having four different emission colors. As presented in Fig. 3, four primary antibodies were found to selectively bind to MCF-7 cancer cell markers (EpCAM, CD44, Keratin 18, and anti-IGF-I) providing excellent cell labeling. (Supplementary Fig. S8 for flow cytometry data.) Additional protein array studies were performed to prove the specificity of the four chosen markers (after binding to the AuNR/Ag) for the MCF-7 cells. (Supplementary Fig. S9.)

SEM and TEM analyses, performed on MCF-7 cells incubated for 30 minutes with the four conjugated AuNR/Ag, indicated

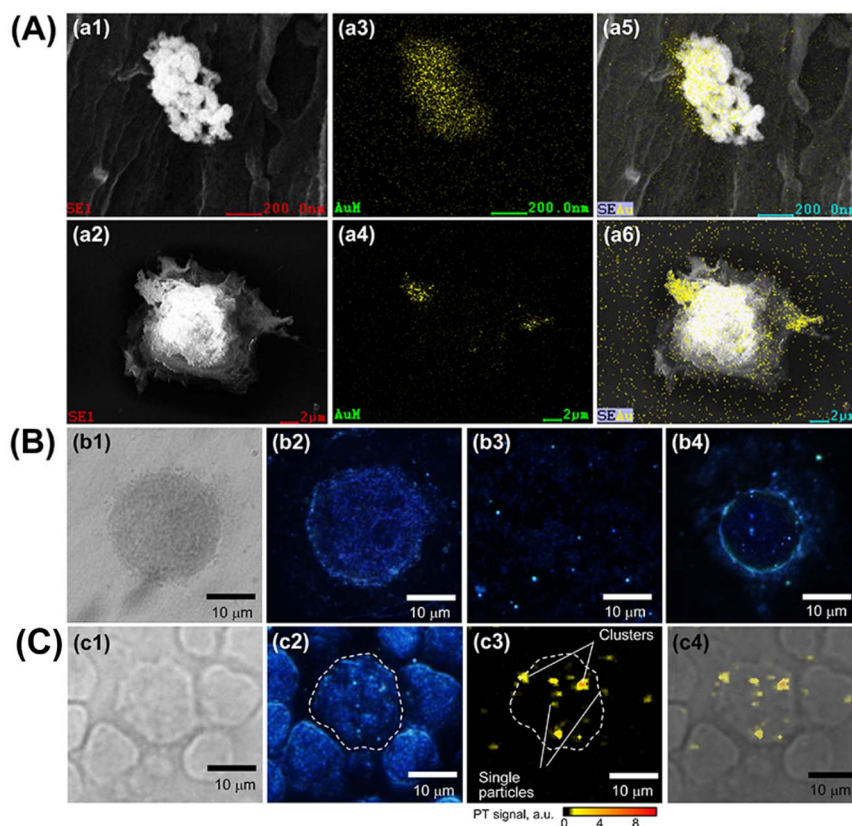


**Figure 4** | Visualization of SERS nanoparticles on the cell membrane surface using: (A) SEM (a1, a2) with EDS Au elemental mapping (a3, a4) confirming AuNR/Ag clustering on the cell surface with the merged SEM and EDS mapping images (a5, a6). (B) Transmission (b1) and EDFM (b2) images of a control MCF-7 cell without SERS Nanorods; EDFM imaging of SERS Nanorods in solution (b3) and on MCF-7 cell membrane in PBS (b4). (C) Multimodal Transmission, EDFM, and PTM imaging of SERS labeled MCF-7 cells among WBCs from separated whole blood (c1),(c2),(c3); Merged PT and transmission microscopy images of the cells with the SERS nanorods on the cellular membranes (c4). PT microscopy parameters: 532 nm, 100 mJ/cm<sup>2</sup>.



that they were preferentially accumulated on the cells (Fig. 4 A, Supplementary Fig. S10 and S11). To further confirm labeling of the cancer cells by the four SERS nanoparticles, we visualized them using enhanced dark-field microscopy (EDFM), Fig. 4B. (See Method section.) As shown in Fig. 4B (b4), the AuNR/Ag accumulated on the surface of MCF-7 cells within 30 minutes of incubation time. In order to verify the specificity of targeting cancer cells in real

human blood samples,  $7 \times 10^6$  WBCs and 100  $\mu$ l of whole unprocessed healthy human blood from volunteers were spiked with 50 MCF-7 cells. The four different SERS AuNR/Ag nanoagents of 50  $\mu$ g/ml (12.5  $\mu$ g/ml of each) were added to the spiked blood samples and incubated for 30 minutes. PTM and EDFM images (Fig. 4 c2–c4) revealed that the SERS AuNR/Ag nanoagents targeted the MCF-7 cells but not the blood cells. Fig. 5A (a1) shows multicolor

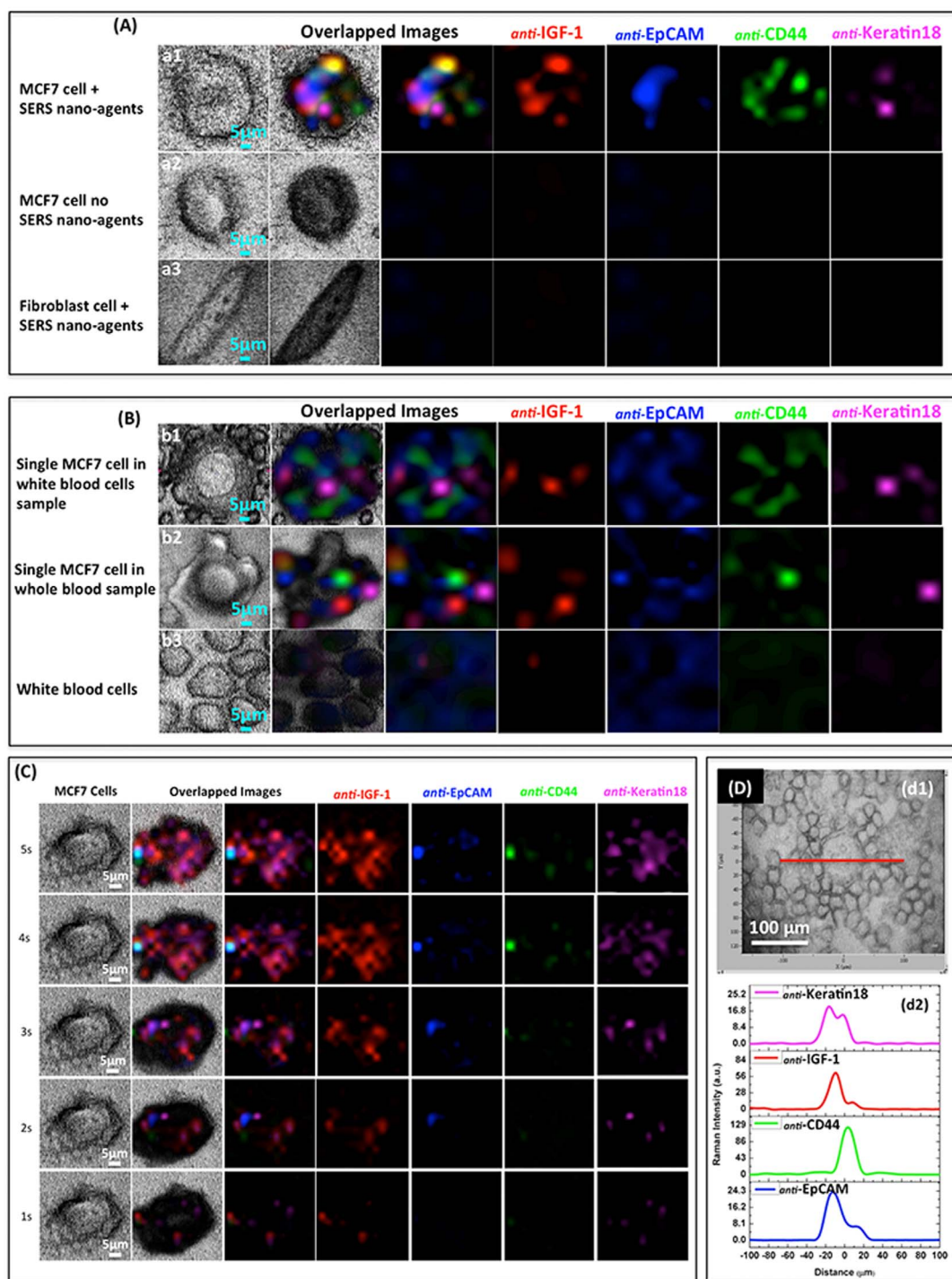


**Figure 5** | (A) Transmission and Raman imaging of a sample containing just one MCF-7 cell among 90,000 fibroblast cells: (a1) MCF-7 cell after 30 min incubation of the sample with four SERS nano-agent cocktail; (a2) control cells, with no SERS nano-agents; (a3) normal fibroblast cell after 30 min incubation with SERS cocktail. (B) Multicolor SERS analysis of MCF-7 cells in blood: (b1) A single MCF-7 cell among WBCs, after 30 min incubation with SERS cocktail; (b2) a single MCF-7 cell in whole (unprocessed) blood, 30 min incubation with SERS cocktail; (b3) WBCs only, 30 min incubation with SERS cocktail, no specific Raman signals were observed. (C) SERS multicolor mapping of single MCF-7 cell at different acquisition times (1–5 seconds), 30 min SERS cocktail incubation. (D) SERS line scan (200  $\mu$ m) across a single MCF-7 cell among white blood cells; (d1) transmission image, (d2) Line scan data interpretation for individual SERS nano-agents.



2-D SERS mapping of a single MCF7 cancer cell co-cultured *in vitro* with fibroblast cells (used as a control for a noncancerous cell line) and incubated with the AuNR/Ag with the four different SERS spectra nanoagents. Fig. 5A (a2) presents the spectral SERS mapping image of a cancer cell that was not incubated with nanoparticles, and Fig. 5A (a3) presents a fibroblast cell incubated with the AuNR/Ag with the four SERS nanoagents. (Supplementary Fig. S12.) Neither of these two measurements provided SERS signals in any spectroscopic region. Fig. 5B (b1) and (b2) demonstrate the results of the 2-D multispectral SERS mapping of one of the 50 MCF-7 cancer cells spiked into  $\sim 7 \times 10^6$  WBCs and whole blood, respectively. The four colors were easily distinguished despite the complex biological background. Fig. 5B, b3 demonstrates the 2-D SERS mapping of WBCs only (without cancer cells) with no specific Raman signals in the four spectral ranges (Supplementary Fig. S13, S14, and S15). These Raman images clearly confirmed that all four SERS nanoagents targeted the same MCF-7 cell, within 30 min incubation. Cell scanning at different acquisition times (1–8 sec) revealed that the SERS signal intensity increased with the acquisition time, reaching a detectable level at 3 sec (Fig. 5C). In addition, SERS mapping of a single cancer cell in the four specific spectroscopic ranges revealed that the four spectrally-different SERS signals were localized in the MCF-7 cell only with no significant signals from blood cells (Fig. 5D, d1–d2). To ensure that the AuNR/Ag nanoagents did not target the blood cells, we conjugated the nanorods with antibodies specific to WBC receptor CD45. AuNR/Ag/4ADPS/CD45 labels (50  $\mu\text{g}/\text{ml}$ ) were incubated for 30 minutes with the WBCs spiked with MCF-7 at different numbers (10, 100, 1000, 10000). As shown in Supplementary Fig. S16A, the 2D SERS mapping indicated that no signal was measured from the MCF-7 cells while the SERS signals came from the WBCs only. Additionally, EDFM and PTM imaging (Supplementary Fig. S16B) confirmed these results.

## Discussion

We demonstrated the multiplex targeting and imaging with multi-color identification of single cancer cells in blood using multimodal optical techniques such as SERS, PTM, and EDFM. We presented a technology for the multiplex detection of tumor cells in whole human blood using tunable, silver-decorated, gold nanorods as SERS multispectral contrast agents, functionalized with four Raman molecules and four antibodies cancer markers—anti-EpCAM, anti-IGF-1 Receptor  $\beta$ , anti-CD44, anti-Keratin18, as well as leukocyte-specific marker anti-CD45. Moreover, these multimodal nanoparticles demonstrated simultaneous multicolor SERS and PT-based super image resolution. Using the proposed antibody cocktail, high specificity was demonstrated for targeting breast cancer cells, used as a CTC model, compared to normal tissue and blood cells. High detection specificity was demonstrated by integrating multiplex targeting, spectroscopic signal amplification, multimodal detection, and 2D multispectral mapping. Furthermore, our approach has the potential to distinguish specific and nonspecific binding, eliminate complex blood processing, and enhance spectral recognition by using non-overlapping, ultra-sharp SERS multispectral 2D mapping and PT plasmonic resonances<sup>6,7</sup>.

The interaction of laser radiation with non-fluorescent plasmonic nanoparticles was detected through Raman or Mie scattering or non-radiative transformation of absorbed energy in heat. However, the conventional Mie scattering and absorption spectra of the nanoparticles are typically very wide, allowing limited spectral identification. We showed a way to enhance the spectral selectivity of cancer diagnostics by integration of narrow, multiple, nonlinear, and sharp SERS/PT resonances<sup>7</sup>, potentially allowing a further increase in the number of colors and hence the nanoparticles' multiplex capability. Super-contrast SERS and PT methods using the same multimodal, tunable AuNR/Ag nanoparticles ideally supplemented each other for cancer cell identification. PT microscopy provides a unique oppor-

tunity to enhance the speed of sample analysis through rapid screening using pulsed PT excitation and swift signal acquisition approaches. In this work, we developed four families of low toxicity (Supplementary Fig. S17) nanostructures based on silver-coated AuNRs—each with a unique Raman molecule and molecular ligands and with super bright spectral Raman signatures to enhance sensitivity and lower detection time. Individual peaks of the four organic molecules' spectra were assigned different colors, and they were used to map, both in 1- and 2-D, the blood samples spiked with the MCF-7 cells used as a CTC model. The presence of all four colors superimposed on the optical images of a cell clearly indicated that the particular cell was a CTC. We further multiplexed the multicolor SERS approach (Raman detection) with a combination of PTM and EDFM.

It should be mentioned that, based on our observations, the AuNR/Ag were found to agglomerate on the membrane of the cells (Figure 4 A and B), which in fact was observed to increase the intensity of both SERS and PT signatures (Supplementary Fig. S18). For both of these techniques, our preliminary analysis indicated non-linear correlations between the spectroscopic signal intensity and the size of the AuNR/Ag clusters. Although the overall detection time required for the analysis of the samples is relatively short, one significant issue could be the state of the Ag layer. As seen from our XPS analysis, the Ag was found to be in a metallic state, and the Raman signature was preserved over a long period of time and consecutive repetitive laser exposures (Supplementary Fig. S19 and Fig. S20).

Our approach allowed the detection with extremely high specificity of a single cancer cell within 7 millions of blood cells without any enrichment or separation or tedious, time-consuming procedures used in other methods<sup>33</sup>. In the future, we plan to extend this technology to further decrease the total analysis time. This swift and accurate identification technique could have critical importance for the early detection of CTCs and subsequent well-timed cancer treatment.

## Methods

**Synthesis of AuNRs.** AuNRs were prepared according to the silver ion-assisted, seed-mediated method developed by Nikoobakht<sup>34</sup>. Briefly, the seed solution was first prepared by mixing 5 ml of CTAB solution (0.2 M) with 5 ml of  $\text{HAuCl}_4$  (0.0005 M), then 600  $\mu\text{l}$  of  $\text{NaBH}_4$  (0.01 M) were added with stirring for two minutes. To synthesize gold nanorods with an aspect ratio of around 3, 5 ml of CTAB (0.2 M) were mixed with 150  $\mu\text{l}$  of silver nitrate solution (0.004 M), then 5 ml of  $\text{HAuCl}_4$  (0.001 M) were added and mixed. Afterward, 70  $\mu\text{l}$  of ascorbic acid 0.0788 M were mixed with the solution, and finally 12  $\mu\text{l}$  of seed solution were added. The mixed solution was kept at 30°C for 40 minutes without any further stirring. AuNRs were further purified twice by centrifugation at 10,000 rpm for 30 min to remove any excess reagents.

**Coating of AuNRs with a thin silver layer.** Prepared gold nanorods were covered with silver layers, using the previously reported method<sup>31,35</sup>. Purified AuNRs were re-dispersed in 5 ml CTAB solution by sonication, and then 5 ml of 1% PVP solution and 250  $\mu\text{l}$  of  $\text{AgNO}_3$  (0.001 M) were added with gentle mixing. Afterward, 100  $\mu\text{l}$  of ascorbic acid (0.1 M) were added, and then 200  $\mu\text{l}$  of NaOH solution (0.1 M) were added to elevate the pH to 9 to initiate the silver ion reduction reaction. Silver-coated gold nanorods (AuNR/Ag) were purified twice by centrifugation at 12,000 rpm and re-dispersed in DI water to remove any excess reagents.

**Assembling SERS probes on the surface of AuNR/Ag.** Four thiophenol derivatives were prepared with 10 mM each ethanol stock solution, in five separate conical flasks, each containing 5 ml of AuNR/Ag<sup>36</sup>. 5  $\mu\text{l}$  each of 4MBA, PATP, PNTP, 4MSTP, and 4ADPS were added and kept under stirring for 3 hours at 45°C. Excess chemicals were removed by centrifugation at 10,000 rpm for 30 min.

**Conjugation of AuNR/Ag with antibodies.** All of the precipitate SERS probe solution was redispersed in 2 ml of HS-PEG-COOH (MW = 3000) solution (2 mg dissolved in 2 mM of NaCl solution) and vigorously stirred for 15 min. 1.8 ml of HS-PEG (2 mg/ml in 2 mM NaCl solution) stabilizer were added and kept in contact with the SERS nano-agents at 5°C for overnight. The unbound thiolated PEG was removed by centrifugation at 4000 rpm for 15 min twice. A two-step NHS/EDC conjugation assay<sup>37</sup> was followed to bind the carboxylated PEG-covered nanorods (SERS nanorods) with the corresponding antibody.



4 ml of purified carboxylated SERS nanorods were conjugated with a certain amount of corresponding antibody to obtain the five different mixtures: anti-EpCAM to AuNR/Ag/4MBA, anti-CD44 to AuNR/Ag/PATP, anti-IGF-1 receptor to AuNR/Ag/PNTP, Keratin18 to AuNR/Ag/AMSTP, and anti-CD45 to AuNR/Ag/4ADPS. The antibody-tagged nanorods (SERS nano-agents) were washed and re-suspended in 5 ml of 1× PBS solution and kept under  $-20^{\circ}\text{C}$ .

**Targeting assay based on SERS nano-agents.** Mixtures of the cancerous MCF-7 cell line and BJ-1 fibroblast cell line were seeded in 4-well chamber slides at a density of  $10^5$  cells/well and a percentage of 90% BJ-1 cells, 10% MCF-7 cells. The cells were supplemented with complete growth medium and incubated overnight for attachment. Post incubation, the medium was changed with normal growth medium supplemented by 40  $\mu\text{g/ml}$  of SERS nano-agents (10  $\mu\text{g}$  of each SERS nano-agents), and the cells were further incubated for 30 min at  $37^{\circ}\text{C}$ . The cells were washed for 5 min 3 times with 1× PBS, and 2% formaldehyde was added for fixation. After 20 min, the cells were washed 6 times (3 times with 1× PBS, 3 times with DI water). The cells were left to dry and stored at  $-20^{\circ}\text{C}$ . Untreated cells were used as a negative control.

SERS images were collected from the samples using a Confocal Raman spectrometer (Horiba Jobin Yvon LabRam HR800, Edison, New Jersey) assembled with He-Ne laser (784 nm) and Olympus BX-51 lens with 100× micro-objective magnitudes connected to a Peltier-cooled CCD camera. The spectra were collected using 600-line/mm gratings with the same acquisition time (8 sec). All data were baselined and background-corrected, then re-constructed using OriginLab software. The spectrometer also has a three-dimensional (3-D) (x-y-z) automatic adjustable stage that can map Raman scanning for a specific area at a minimum distance of 1  $\mu\text{m}$ . In all measurements, the Raman spectrometer was calibrated using the Si-Si Raman signal, which is located at a  $521\text{-cm}^{-1}$  Raman shift.

Blood samples were drawn from healthy donors under the approved IRB protocol in place at UAMS. Two sets of blood samples were used in this study: whole blood and separated white blood cells (WBCs). All specimens were collected into vacutainer blood collection tubes containing the anticoagulant EDTA and were used within the first few hours. The WBCs were separated by following the Lymphoprep™ (Fisher Scientific) procedure for human mononuclear cell separation. Briefly, 1 ml of the whole blood was first mixed in 1:1 v/v ratio with 1× PBS solution in separate tubes and was added carefully on top of 1 ml of lymphoprep solution. Following centrifugation at 2000 rpm for 30 minutes, the middle layer was collected, and the cells were washed and centrifuged 3 times with 1× PBS. The pellets were finally re-suspended with 100  $\mu\text{l}$  of PBS. The desired numbers of MCF-7 cells (10, 100, 1000, 10000) were spiked with blood samples and SERS nano-agents in a concentration of 50  $\mu\text{g/ml}$  (12.5  $\mu\text{g}$  of each SERS nano-agent), then added to the samples and incubated for 30 min at  $37^{\circ}\text{C}$ . After incubation, 100  $\mu\text{l}$  of each sample were placed in the Cytospin in order to obtain a monolayer of cells on a glass slide. The same assays of fixation and Raman measurement were conducted as described in the previous section.

**Photothermal (PT) microscopy and enhanced dark field microscopy (EDFM).** The PT microscopy schematic has been previously described in detail<sup>1,7,38,39</sup>. The PTM was built on the technical platform of an Olympus IX81 inverted microscope (Olympus America, Inc., Central Valley, PA) with the use of a tunable optical parametric oscillator (OPO; Opolette HR 355 LD, Oportek, Inc., Carlsbad, CA) having a 5-ns wide laser pulse, a repetition pulse rate of 100 Hz, a wavelength range of 410–2,500 nm, and a fluence range of 1–10<sup>4</sup> mJ/cm<sup>2</sup>. The He-Ne laser (model 117A, Spectra-Physics, Inc., Stahnsdorf, Germany; wavelength, 633 nm; power, 1.4 mW) collinear with the excitation OPO beam probed thermal effects in the sample. Excitation and probe beams were focused into the sample by a 40× objective (Ach 40, NA 0.65, Olympus America, Inc.). The probe beam after sample was collected by a 40× long working distance objective (Nikon Ph3 DL, NA 0.55, Tokyo, Japan) and focused by a 25-mm lens on a 200- $\mu\text{m}$  pinhole confocal with the sample plane. The total probe beam power was 30–130  $\mu\text{W}$  in the sample plane. To create a PT image, the sample was raster scanned with XY stage (HI17 ProScan II, Prior Scientific, Inc., Rockland, MA) with a 500 nm step size. Laser-induced, temperature-dependent variations of the refractive index around absorbing zones provided a decrease in probe beam intensity, which was detected by a fast photodetector (PDA10A, Throlabs, Inc, Newport, NJ). PT spectra were acquired from the sample by tuning OPO wavelength and acquiring PT signals from the same sample spot and normalizing the signals on laser pulse energy. PT signals were recorded by a 200-MHz analog-to-digital converter board (PCI-5152, National Instruments Corp., Austin, TX) and analyzed by custom software (LabVIEW 2012; National Instruments). A Dell Precision 690 workstation provided signal acquisition/processing, synchronization of the excitation laser, and translation-stage control. Moreover, nonlinear nanobubble-associated PT signal enhancement makes it possible to circumvent the diffraction limit, for super-resolution imaging of clustered nanoparticles<sup>2</sup>. To perform sample imaging in EDFM mode, an enhanced illuminator (CytoViva Inc., Auburn, AL) replaced a custom 40× objective used for PT imaging. The illuminator consisted of a CytoViva 150 condenser and fiber optic light guide connected to a Solarc 24 W metal halide light source (Welch Allyn, Skaneateles Falls, NY). The sample image was acquired using a 100× oil objective with an iris (Olympus UPlanAPO fluorite, N.A. 1.35–0.55) by a high-resolution color camera (DP72, Olympus America Inc.). The EDFM illuminator dramatically increases the contrast of nano-sized light scattered nanoparticles inside cells<sup>40</sup>.

1. Kuo, A. H. & Clarke, M. F. Identifying the metastatic seeds of breast cancer. *Nat Biotech* **31**, 504–505 (2013).

2. Yu, M. *et al.* Circulating breast tumor cells exhibit dynamic changes in epithelial and mesenchymal composition. *Science* **339**, 580–584 (2013).
3. Nagrath, S. *et al.* Isolation of rare circulating tumour cells in cancer patients by microchip technology. *Nature* **450**, 1235–1239 (2007).
4. Galanzha, E. I. *et al.* In vivo magnetic enrichment and multiplex photoacoustic detection of circulating tumour cells. *Nat Nano* **4**, 855–860 (2009).
5. Stott, S. L. *et al.* Isolation of circulating tumor cells using a microvortex-generating herringbone-chip. *Proc Natl Acad Sci U.S.A.* **107**(43), 18392–18397 (2010).
6. Ozkumur, E. *et al.* Inertial focusing for tumor antigen-dependent and -independent sorting of rare circulating tumor cells. *Sci Transl Med* **5** (179), 179ra47 (2013).
7. Zharov, V. P. Ultrasharp nonlinear photothermal and photoacoustic resonances and holes beyond the spectral limit. *Nat Photon* **5**, 110–116 (2011).
8. Gaiduk, A., Yorulmaz, M., Ruijgrok, P. V. & Orrit, M. Room-temperature detection of a single molecule's absorption by photothermal contrast. *Science* **330**, 353–356 (2010).
9. Nedosekin, D. A., Galanzha, E. I., Dervishi, E., Biris, A. S. & Zharov, V. P. Super-resolution nonlinear photothermal microscopy. *Small*, DOI: 10.1002/smll.201300024 (2013).
10. Vo-Dinh, T., Wang, H.-N. & Scaffidi, J. Plasmonic nanopores for SERS biosensing and bioimaging. *J Biophoton* **3**, 89–102 (2010).
11. Qian, X. *et al.* In vivo tumor targeting and spectroscopic detection with surface-enhanced Raman nanoparticle tags. *Nat Biotech* **26**, 83–90 (2008).
12. Alivisatos, P. The use of nanocrystals in biological detection. *Nat Biotech* **22**, 47–52 (2004).
13. Gao, X., Cui, Y., Levenson, R. M., Chung, L. W. K. & Nie, S. In vivo cancer targeting and imaging with semiconductor quantum dots. *Nat Biotech* **22**, 969–976 (2004).
14. Masilamani, V., Al-Zhrani, K., Al-Salhi, M., Al-Diab, A. & Al-Ageily, M. Cancer diagnosis by autofluorescence of blood components. *Journal of Luminescence* **109**, 143–154 (2004).
15. Sha, M. Y., Xu, H., Natan, M. J. & Cromer, R. Surface-enhanced Raman scattering tags for rapid and homogeneous detection of circulating tumor cells in the presence of human whole blood. *JACS* **130**, 17214–17215, doi:10.1021/ja804494m (2008).
16. Nolan, J. P. *et al.* Single cell analysis using surface enhanced Raman scattering (SERS) tags. *Methods* **57**, 272–279 (2012).
17. Scheidegger, K. J., Cenni, B., Picard, D. & Delafontaine, P. estradiol decreases IGF-1 and IGF-1 receptor expression in rat aortic smooth muscle cells: mechanisms for its atheroprotective effects. *J. Biol Chem* **275**, 38921–38928 (2000).
18. Adams, T. E., Epa, V. C., Garrett, T. P. J. & Ward\*, C. W. Structure and function of the type 1 insulin-like growth factor receptor. *Cell. Mol. Life Sci.* **57**, 1050–1093, doi:10.1007/pl00000744 (2000).
19. Papa, V. *et al.* Insulin-like growth factor-I receptors are overexpressed and predict a low risk in human breast cancer. *Cancer Res* **53**, 3736–3740 (1993).
20. Chang, L. & Goldman, R. D. Intermediate filaments mediate cytoskeletal crosstalk. *Nat Rev Mol Cell Biol* **5**, 601–613, doi:10.1038/nrm1438 (2004).
21. Al-Hajj, M., Wicha, M. S., Benito-Hernandez, A., Morrison, S. J. & Clarke, M. F. Prospective identification of tumorigenic breast cancer cells. *PNAS* **100**, 3983–3988 (2003).
22. Goodison, S., Urquidí, V. & Tarin, D. CD44 cell adhesion molecules. *Mol. Pathol.* **52**, 189–196 (1999).
23. Armstrong, A. & Eck, S. L. EpCAM: A new therapeutic target for an old cancer antigen. *Cancer Biol. Ther.* **2**, 320–325 (2003).
24. Baeuerle, P. A. & Gires, O. EpCAM (CD326) finding its role in cancer. *Br J Cancer* **96**, 417–423 (2007).
25. Went, P. T. H. *et al.* Frequent EpCam protein expression in human carcinomas. *Hum. Pathol.* **35**, 122–128 (2004).
26. Masilamani, V., Al-Zhrani, K., Al-Salhi, M., Al-Diab, A. & Al-Ageily, M. Cancer diagnosis by autofluorescence of blood components. *J. Lumin.* **109**, 143–154 (2004).
27. Zavaleta, C., Smith, B. R., Ian Walton, William Doering, Glenn Davis, Borzoyeh Shojaei, Natan, M. J. & Gambhir, S. S. Multiplexed imaging of surface enhanced Raman scattering nanotags in living mice using noninvasive Raman spectroscopy. *PNAS* **106**, 13511–13516 (2009).
28. Parisot, J. P., Hu, X. F., DeLuise, M. & Zalberg, J. R. Altered expression of the IGF-1 receptor in a tamoxifen-resistant human breast cancer cell line. *Br J Cancer* **79**, 693–700, doi:10.1038/sj.bjc.6690112 (1999).
29. Turner, B. C. *et al.* Insulin-like growth factor-I receptor overexpression mediates cellular radioresistance and local breast cancer recurrence after lumpectomy and radiation. *Cancer Res* **57**, 3079–3083 (1997).
30. Jana, N. R., Gearheart, L. & Murphy, C. J. Wet chemical synthesis of high aspect ratio cylindrical gold nanorods. *J. Phys. Chem. B* **105**, 4065–4067, doi:10.1021/jp0107964 (2001).
31. Liu, M. & Guyot-Sionnest, P. Synthesis and optical characterization of Au/Ag core/shell nanorods. *J. Phys. Chem. B* **108**, 5882–5888, doi:10.1021/jp037644o (2004).
32. Jana, N. R. & Pal, T. Anisotropic metal nanoparticles for use as surface-enhanced Raman substrates. *Adv. Mater.* **19**, 1761–1765, doi:10.1002/adma.200601749 (2007).
33. Chung, Y.-K. *et al.* An electrical biosensor for the detection of circulating tumor cells. *Biosens. Bioelectron.* **26**, 2520–2526, doi:10.1016/j.bios.2010.10.048 (2011).



34. Nikoobakht, B. & El-Sayed, M. A. Preparation and growth mechanism of gold nanorods (NRs) using seed-mediated growth method. *Chem. Mater.* **15**, 1957–1962, doi:10.1021/cm020732l (2003).
35. Becker, J. *et al.* Plasmonic focusing reduces ensemble linewidth of silver-coated gold nanorods. *Nano Lett* **8**, 1719–1723, doi:10.1021/nl080720k (2008).
36. Michota, A. & Bukowska, J. Surface-enhanced Raman scattering (SERS) of 4-mercaptobenzoic acid on silver and gold substrates. *J. Raman Spectrosc.* **34**, 21–25, doi:10.1002/jrs.928 (2003).
37. Kulin, S., Kishore, R., Hubbard, J. B. & Helmerson, K. Real-time measurement of spontaneous antigen-antibody dissociation. *Biophys. J.* **83**, 1965–1973 (2002).
38. Nedosekin, D. A., Galanzha, E. I., Ayyadevara, S., Shmookler Reis, Robert, J. & Zharov, V. P. Photothermal confocal spectromicroscopy of multiple cellular chromophores and fluorophores. *Biophys. J.* **102**, 672–681 (2012).
39. Nedosekin, D. A., Shashkov, E. V., Galanzha, E. I., Hennings, L. & Zharov, V. P. Photothermal multispectral image cytometry for quantitative histology of nanoparticles and micrometastasis in intact, stained and selectively burned tissues. *Cytometry Part A* **77A**, 1049–1058, doi:10.1002/cyto.a.20977 (2010).
40. Grabinski, C. *et al.* Effect of gold nanorod surface chemistry on cellular response. *ACS Nano* **5**, 2870–2879, doi:10.1021/nn103476x (2011).

## Acknowledgments

The work was supported by Arkansas Science and Technology Authority (ASTA) grant (08-CAT-03) and the US Army TATRC program. This work was partly supported by grants from the National Institutes of Health (RO1CA131164, RO1EB009230, R01DK078908, P20RR016460 and P20GM103429) the National Science Foundation (DBI-0852737), the Department of Defense (W81XWH-11-1-0123), the Arkansas Breast Cancer Research Program Grant G1-40728-01, as well as grants from the Arkansas Bioscience Institute and the Translational Research Institute at the University of Arkansas for Medical Sciences. We

acknowledge the contributions of Dr. Huilu Yao to the PT analysis of the samples. The editorial assistance of Dr. Marinelle Ringer is also acknowledged.

## Author contributions

Z.A.N. and Y.X. synthesized the nanomaterials and collected, interpreted optical absorption and Raman data; M.M. and E.I.G. designed and collected the data related to marker targeting; T.M. and F.W. performed microscopy and XPS analysis; D.A.N. performed PT/EDFM imaging; M.A.J. handled blood samples and performed EDFM imaging; H.Y. explored PT resonances; J.P.N. provided reference gold nanorods for PT/Raman; T.F. and A.G.B. designed and performed studies related to the specificity/toxicity of the nanorods, V.P.Z. designed PT related research, analyzed the data; A.S.B. designed experiments, analyzed data; Z.A.N., Y.X., M.M., V.P.Z., F.W., A.B. and A.S.B. co-wrote the paper.

## Additional information

**Supplementary information** accompanies this paper at <http://www.nature.com/scientificreports>

**Competing financial interests:** The authors declare no competing financial interests.

**How to cite this article:** Nima, Z.A. *et al.* Circulating cancer cell identification by functionalized silver-gold nanorods with super-enhanced SERS and photothermal resonances. *Sci. Rep.* **4**, 4752; DOI:10.1038/srep04752 (2014).



This work is licensed under a Creative Commons Attribution-NonCommercial-NoDerivs 3.0 Unported License. The images in this article are included in the article's Creative Commons license, unless indicated otherwise in the image credit; if the image is not included under the Creative Commons license, users will need to obtain permission from the license holder in order to reproduce the image. To view a copy of this license, visit <http://creativecommons.org/licenses/by-nc-nd/3.0/>